

Cr/S/TiO₂-LOADED HOLLOW GLASS MICROSPHERES AS AN EFFICIENT AND RECYCLABLE CATALYST FOR THE PHOTOCATALYTIC DEGRADATION OF INDIGO CARMINE UNDER VISIBLE LIGHTXiuli Zhang^a, Yidong Yin^{a,*}, Zhibo Sun^a, Yingqiu Du^b, Shichao Ma^a and Yan Wu^a^aSchool of Chemistry and Materials Science, Heilongjiang University, Harbin 150080, Nangang, P. R. China^bAgricultural Products Quality and Safety Research Institute, Heilongjiang Academy of Agricultural Sciences, Harbin 150086, Nangang, P. R. China

Recebido em 05/01/2016; aceito em 05/04/2016; publicado na web em 13/07/2016

Chromium and sulfur co-doped nanometer TiO₂ hollow glass microspheres (Cr/S/TiO₂-HGM) were synthesized by a sol-gel method. Characterization used X-ray diffraction (XRD), scanning electron microscopy (SEM), energy-dispersive X-ray spectroscopy (EDX), N₂ adsorption-desorption (Brunauer-Emmett-Teller (BET) measurements) and UV-Vis diffuse reflectance spectroscopy. The photocatalytic activity was evaluated by photodegradation of indigo carmine in an aqueous solution under visible light irradiation. The results indicated that the Cr/S/TiO₂ containing 0.60% (atomic ratio) chromium and 1.2% (atomic ratio) sulfur calcined at 500 °C for 2 h had high catalytic efficiency under visible light irradiation. The floating Cr/S/TiO₂-HGM catalyst had greater photocatalytic activity than Cr/S/TiO₂ powder. Therefore, Cr/S/TiO₂-HGM is a promising, high-performing, visible-light-driven, and more reusable photocatalyst.

Keywords: hollow glass microspheres; visible light; indigo carmine; TiO₂; photocatalytic degradation.

INTRODUCTION

Wastewater from textile industries frequently contains significant amounts of non-biodegradable dyes.¹ Most of these dyes are toxic and potentially carcinogenic, and their removal from industrial effluents is a major environmental concern.² One of the most widely used dyes in the textile industry is indigo carmine or acid blue 74. It is also an additive in pharmaceutical tablets and capsules and used in medical diagnostics.³ However, this highly toxic indigoid class of dye is carcinogenic, and can lead to reproductive, developmental, neuronal and acute toxicity as well as carcinogenesis.⁴ It can also cause mild to severe hypertension and have cardiovascular and respiratory effects in patients.⁵ Thus, the removal of indigo carmine from water and wastewater is very important.

TiO₂ is one of the most promising photocatalysts. It is widely used in wastewater treatment and hydrogen generation.⁶ However, pure bulk TiO₂ is active under ultraviolet light, which is a small part (3-5%) of the solar spectrum. Many different attempts have been made to modify TiO₂ on the surface or in the bulk to make it active with visible light. This is primarily done via ionic doping. Many types of doped TiO₂ materials show varying degrees of photocatalytic activities under visible light irradiation. In some cases, two types of doping ions were introduced simultaneously into TiO₂ to pursue enhanced visible light responses.⁷⁻⁹ So far, there are few reports using Cr/S/TiO₂ as a visible light-activated photocatalyst, which is surprising because Cr/S/TiO₂ extends its absorption to the visible region yet.^{10,11} The Cr/S/TiO₂ heterojunction has a high photocatalytic ability to degrade indigo carmine under visible light.¹²

TiO₂ is an excellent photocatalyst for the removal of organic contaminants from wastewater. However, separation of the TiO₂ particles from the treated water is difficult because the particles are too small to be removed. Therefore, attempts have been made to separate TiO₂ photocatalysts via a variety of supported materials including glass microspheres, graphene, zeolites, and concrete.¹³⁻¹⁶

Hollow glass microspheres (HGM) are widely used in various

fields.¹⁷⁻¹⁹ HGM-TiO₂ is an important composite material and became commercially available. It is easy to separate and recover. Thus, HGM-TiO₂ is promising for use in industrial wastewater treatment plants and the reduction of gaseous pollutants due to its unique properties including low density, buoyancy, and transparency to visible light.¹¹ However, detailed studies on the photocatalytic performance and applications of HGM-TiO₂ have received limited attention.

In this study, a novel chromium and sulfur co-doped TiO₂ photocatalyst was synthesized via a sol-gel method. To improve the separation and adsorption capacity, the photocatalyst was loaded on hollow glass microspheres and can thus be recycled.

EXPERIMENTAL**Materials**

Tetrabutyl titanate, glacial acetic acid and absolute ethanol were purchased from Tianjin Kemiou Chemical Reagent Co., Ltd., China. Potassium persulfate, chromium nitrate nonahydrate, and indigo carmine were purchased from Shanghai Aladdin Industry Co., Ltd., China. Commercial P25 (80% anatase and 20% rutile) was purchased from Degussa (China) Co., Ltd. Other chemicals of analytical grade were used without further purification. Deionized water was used in all experiments. Hollow glass microspheres (H60) were from Beijing Sinosteel Corporation, China.

Sample Preparation

Chromium and sulfur co-doped nanometer TiO₂ supported on hollow glass microspheres (Cr/S/TiO₂-HGM) were prepared by a sol-gel method. To obtain solution A, 8.5 mL tetrabutyl titanate was dissolved in 19.5 mL ethanol absolute, and the mixture stirred for 30 min. Chromium nitrate nonahydrate and potassium persulfate were then dissolved with 9.4 mL deionized water, 10 mL acetic acid glacial and 9.7 mL ethanol absolute to obtain homogeneous solution B. The catalyst is doped with 0.60% chromium and 1.2% sulfur.¹¹ Solution B was then added dropwise to solution A at room temperature with

*e-mail: yin_yidong@sina.com

vigorous stirring for 30 min. Hollow glass microspheres (1:1 weight ratio) were then added to the above solution, and the mixture was stirred for 30 min. The resulting homogeneous green solution was subsequently aged at room temperature for 2 h. The final solution was further dried at 80 °C until a dry Cr/S/TiO₂-HGM was achieved. This was then placed in a muffle furnace. The temperature increased to 300, 400, 500, 600, 700, and 800 °C (100 °C/h) and was held constant for 2 h. The substrates were then cooled (50 °C/h) to room temperature and used for characterization. For comparison, pure TiO₂ and Cr/S/TiO₂ were similarly prepared.

Characterization

The X-ray diffraction (XRD) patterns were collected with a Bruker D8 X-ray Diffractometer using CuK α ($\lambda = 1.5406\text{\AA}$) at a step scan of 0.02° from 10° to 80°. The scanning electron microscopy (SEM) images were recorded with a Hitachi S-4800 field emission scanning electron microscope with primary electron energy of 15 kV. The energy-dispersive X-ray spectroscopy (EDX) attached to the SEM determined the surface elemental composition. The BET surface areas were obtained by N₂ adsorption-desorption surface area (Micromeritics ASAP 2020). All samples were degassed in a vacuum at 473 K for 4 h before measurements. The surface area of the materials was calculated by the Brunauer–Emmett–Teller (BET) theory. The UV-Vis diffuse reflectance spectra were measured using a UV-Vis diffuse reflectance spectrophotometer (UV-Vis DRS: TU-1901, China) equipped with an integrating sphere assembly and BaSO₄ as the reflectance sample. The spectra were recorded at room temperature in air from 200 to 800 nm.

Photodegradation

Photocatalytic experiments used a homemade reactor that was surrounded with a cooling system to maintain room temperature. A 500 W halogen lamp assisted with Toshiba B-47 optical filter ($\lambda > 410$ nm) was used as the visible light source. The catalyst was suspended in 100 mL of an indigo carmine solution (20 mg L⁻¹) under magnetic stirring. The mixture was kept in the dark for 40 min to establish an adsorption-desorption equilibrium before the visible light radiation. At given intervals, 4 mL of suspension was extracted and then centrifuged at 5000 rpm for 3 min to remove the catalysts from the supernatant. The absorbance was then measured at 610 nm using a 721 spectrophotometer. Catalyst was added to a working concentration of 6 g L⁻¹.

RESULTS AND DISCUSSION

Indigo carmine (20 mg L⁻¹) in aqueous solution was photocatalytically degraded with chromium and sulfur co-coated TiO₂ powder catalysts. The Cr/S/TiO₂ photocatalyst contained 0.60% (atomic ratio) chromium and 1.2% (atomic ratio) sulfur; it was calcined at 500 °C for 2 h. More details of the properties of the photocatalysts are given below.

XRD analysis

The XRD patterns of different materials are shown in Figure 1 (a). The patterns contain nine distinctive TiO₂ peaks at 25, 37.80, 48.06, 53.90, 55, 62.7, 68.76, 70.17, and 75.37°. These correspond to the different anatase crystal planes (JCPDS 00-002-0387). This indicates that the synthesized powder is mainly anatase. A comparison of the patterns obtained from TiO₂ and the Cr/S/TiO₂ powders revealed that the diffraction peaks of TiO₂ did not change. The Cr peaks were

not observed because Cr may be located in the interstice of the TiO₂ or enters the crystal lattice instead of Ti. The S atoms may replace some of the oxygen atoms in the TiO₂ crystal lattice. The absence of any sulfur peaks confirms a lack of residual sulfur on the nanocrystal. Figure 1 shows single broad peak of HGM around 22.4°. This indicates the presence of an amorphous nature. The crystal phase of Cr/S/TiO₂ and Cr/S/TiO₂-HGM are anatase TiO₂ indicating that the right amount of loading does not change the crystal structure of the catalyst.

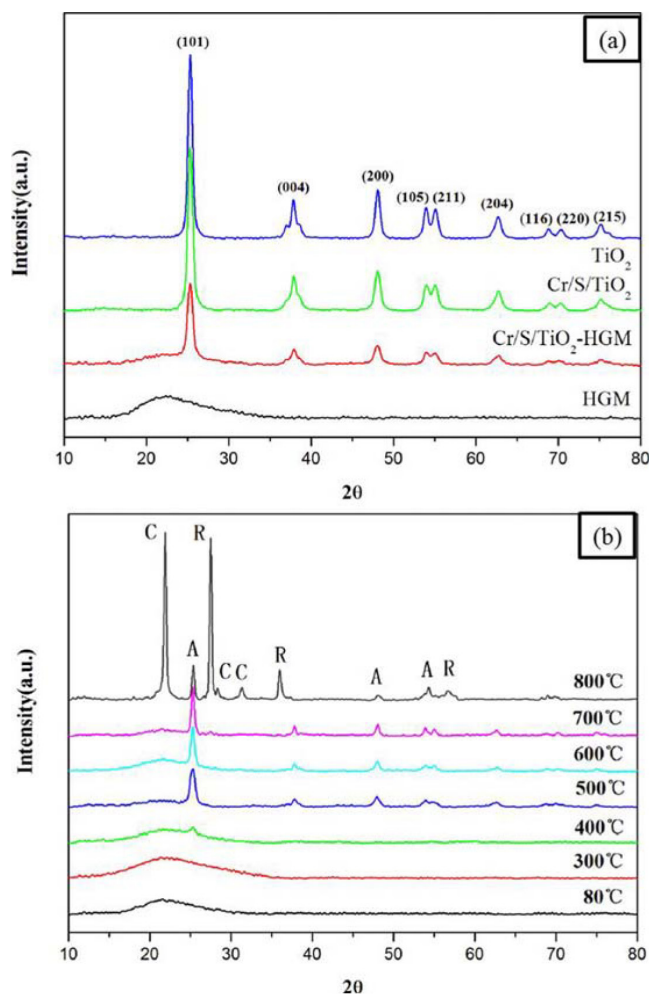


Figure 1. (a) XRD patterns of different materials. (b) XRD patterns of Cr/S/TiO₂-HGM at different temperatures (A: anatase, R: rutile, C: cristobalite)

The HGM surface becomes a dry gel after calcination. It may contain hydrolyzed byproducts from tetrabutyl titanate, ethanol, and water as well as incompletely crystallized TiO₂. Thus, a defined temperature is needed to obtain Cr/S/TiO₂-HGM. The calcination temperature is one of the most important factors affecting Cr/S/TiO₂-HGM photocatalytic activity.

Figure 1 (b) shows the XRD patterns of Cr/S/TiO₂-HGM calcined at different temperatures. The crystal phase was confirmed with JCPDS Card No. 01-078-1508 and 01-074-9378. The samples after calcination at 80 and 300 °C are amorphous TiO₂ and HGM. At 400 °C, there is a small amount of anatase TiO₂ in the sample. When the calcination temperature was between 500–700 °C, the Cr/S/TiO₂-HGM exists mainly as anatase TiO₂ and amorphous HGM. The TiO₂ crystal is stable after loading within this temperature range. Above 800 °C, the Cr/S/TiO₂-HGM is a rutile TiO₂ and cristobalite. Rutile TiO₂ causes the catalyst surface to easily absorb water. This is not

conductive to photocatalysis. The diffraction peaks becomes intense and narrow when the calcination temperature increased. A crystalline structure is gradually formed and crystallites gradually grow.

SEM analysis

Figure 2 shows SEM images of Cr/S/TiO₂-HGM for different loading times. The HGM particle size is in the range of 15-35 μm and can easily be separated from the treated wastewater. The surface after one round of loading (HGM surface with a layer of Cr/S/TiO₂) was characterized (Figure 2 (a)); two rounds of loading are shown in Figure 2 (b, e, f). The TiO₂ film had many fractures on the surface of the HGM. This is due to the gel coat. After drying and calcination, the thin film contracts to make these fractures. This increases the specific surface area of the catalyst and enhances the Cr/S/TiO₂-HGM photocatalytic effect. Three and four rounds of loading are shown in Figures 2 (c) and 2 (d), all of the HGM have different loading thicknesses. Loading too much Cr/S/TiO₂ on the HGM will affect the energy efficiency, and the Cr/S/TiO₂ easily falls off. The optimum number of loading replicates is two.

EDX analysis

The elemental composition of the samples was estimated by EDX.

The SEM and EDX analyses of HGM before and after the loading are shown in Figure 3. Figure 3 (a₂) shows that the HGM are mainly composed of Si and O. The HGM data after loading are shown in Figure 3 (b₂) - this confirms the presence of Ti, Cr, S, Si, and O. The spectra indicate that the main components are Ti and O with low contents of Cr and S. The XRD and EDX data show that the HGM surface is loaded with Cr/S/TiO₂.

UV-Vis DRS analysis

The light absorption characteristics of TiO₂ usually change after doping with nonmetal doping²⁰⁻²² and metal/nonmetal co-doping.²³⁻²⁵ Figure 4 presents the UV-Vis diffuse reflection absorption spectra of TiO₂, Cr/S/TiO₂, and Cr/S/TiO₂-HGM. The absorption wavelength of pure TiO₂ is less than 400 nm, and bulk TiO₂ is a wide band gap semiconductor with a band gap of 3.2 eV (387 nm) for anatase.²⁶ The absorption spectra of the Cr/S/TiO₂ and Cr/S/TiO₂-HGM samples obviously extend deeper into the visible light region relative to TiO₂. Interestingly, the Cr/S/TiO₂ shows significant absorption from 400 to 800 nm. The absorption of light increases dramatically in the visible region¹⁰ after S and Cr co-doping. There is an absorption peak of Cr/S/TiO₂ and Cr/S/TiO₂-HGM around 400-450 nm corresponding to Cr.²⁷ The absorption at 450 nm is assigned to the electron transition in the energy level of doping Cr³⁺. This transfers into the conduction band

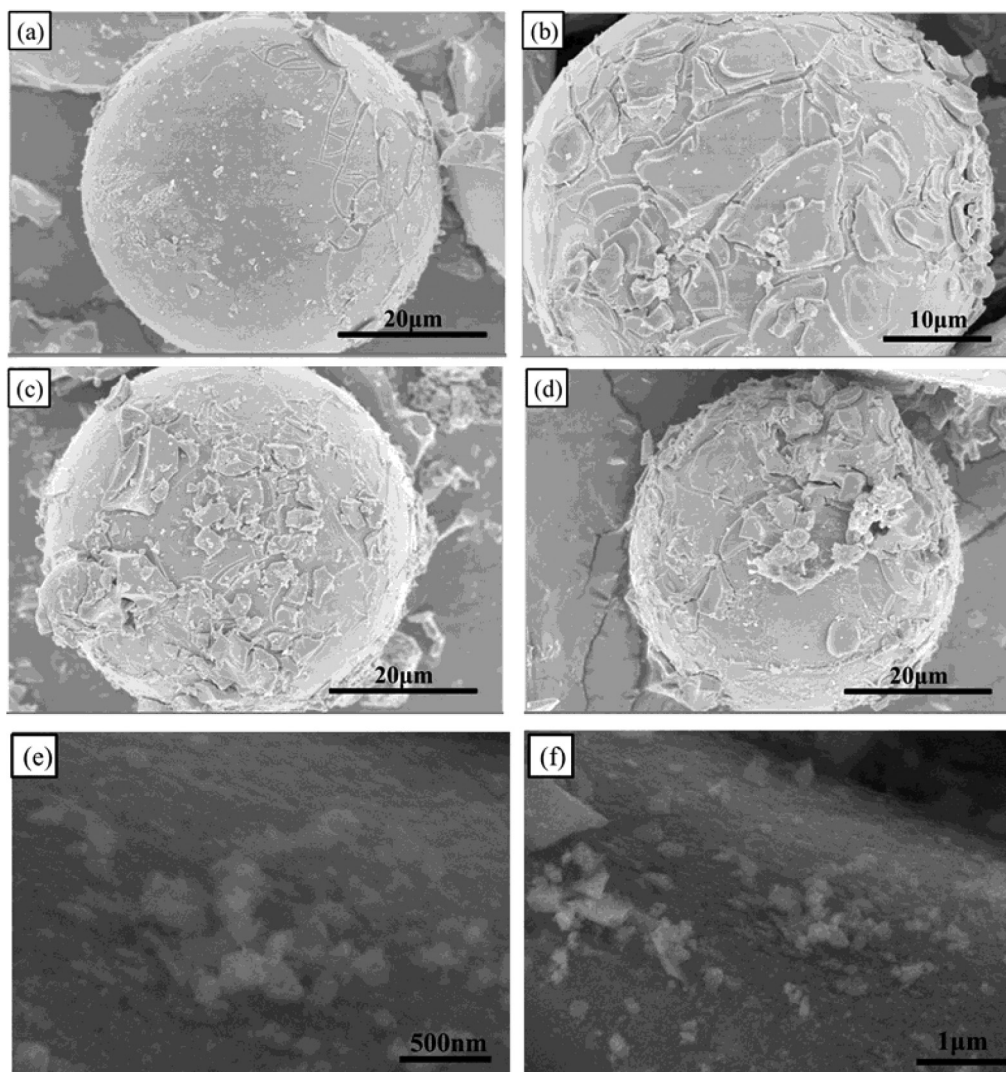


Figure 2. SEM images of Cr/S/TiO₂-HGM with different loading replicates: (a) 1 time, (b, e, f) 2 times, (c) 3 times, and (d) 4 times

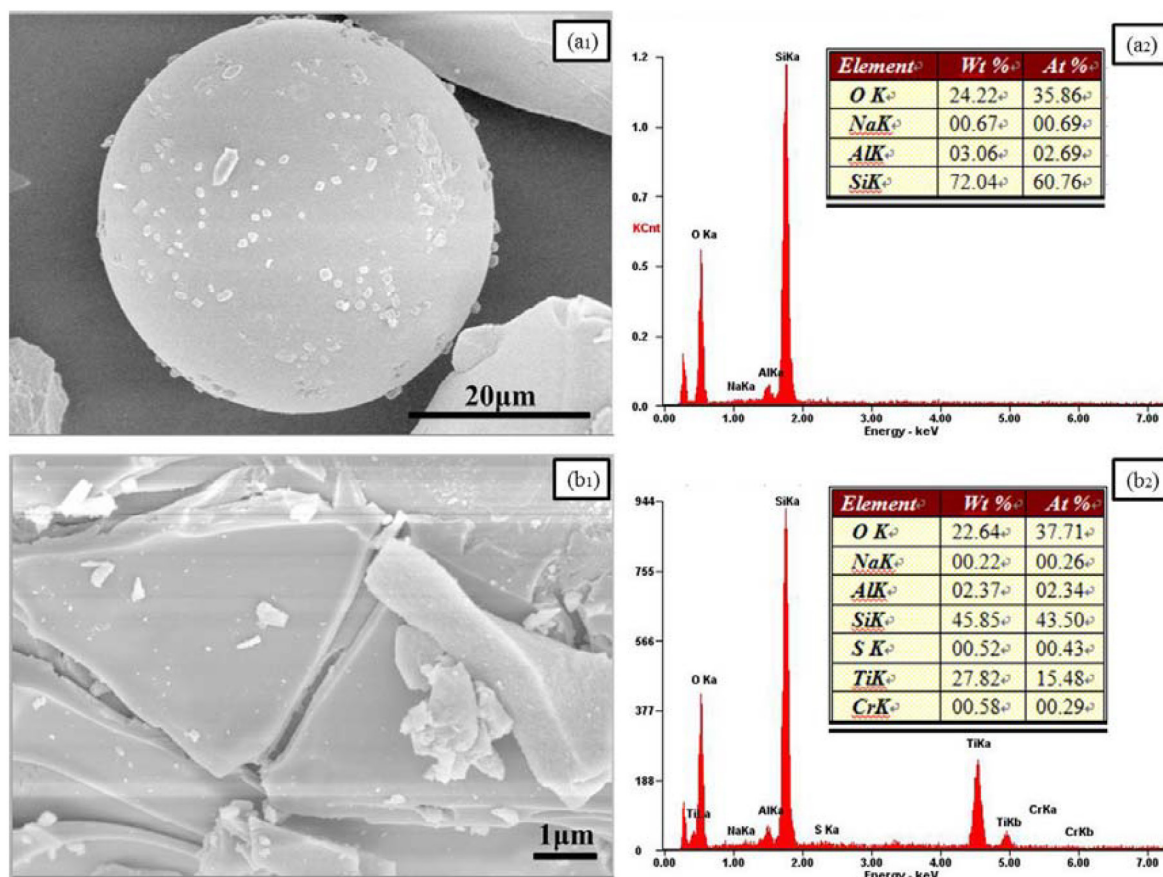


Figure 3. SEM images and EDX spectra of the (a) HGM and (b) Cr/S/TiO₂-HGM

(Cr³⁺→Ti⁴⁺) of TiO₂.¹⁰ Additional absorption is due to the Cr³⁺ ion itself (4A_{2g}→4T_{1g}).²⁸⁻³⁰ There is a wide absorption band in the 620–800 nm range that can be attributed to the d-d transitions (4A_{2g}→4T_{2g}) of Cr³⁺.¹² The Cr/S/TiO₂-HGM shows a broader absorption ranging from UV light to visible light (200–800 nm). Thus, the Cr/S/TiO₂ loaded on hollow glass microspheres enhances catalyst light absorption.

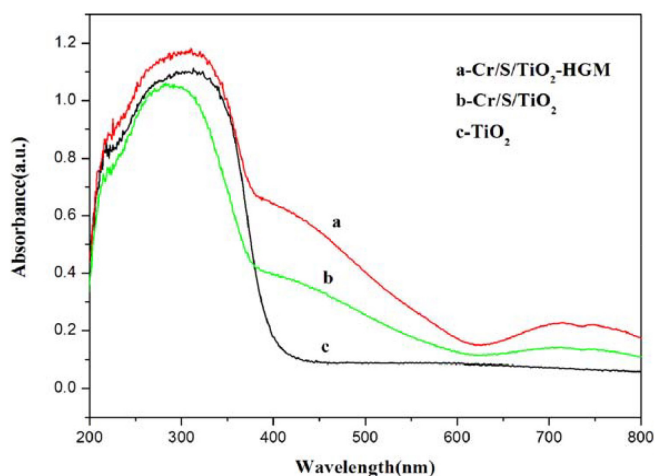


Figure 4. UV-visible spectra of different materials

BET measurements

The BET surface area obtained from the N₂ adsorption–desorption isotherms are listed in Table 1. The BET surface area of the Cr/S/TiO₂ is higher than the TiO₂. The BET surface area increased to 176 m² g⁻¹ after loading. The Cr/S/TiO₂-HGM sample has a high

Table 1. The BET surface area of samples

Sample	BET surface area (m ² g ⁻¹)
TiO ₂	47
Cr/S/TiO ₂	87
HGM	132
Cr/S/TiO ₂ -HGM	176

surface area, and this could enhance the visible absorption and thus photocatalytic activity.

Photocatalytic activity

The photocatalytic activity of all samples is given below. This was evaluated by degradation of indigo carmine under irradiation with visible light. The initial concentration of indigo carmine is 20 mg L⁻¹, and the degradation time is 80 min.

The effect of calcination temperature on the Cr/S/TiO₂-HGM photocatalytic activity

Figure 5 shows the effect of the calcination temperature on the photocatalytic activity. Samples of Cr/S/TiO₂-HGM and their photocatalytic performances are different. The samples calcined at 80, 300 and 400 °C have negligible photocatalytic activity. The photocatalytic activity of the 500 °C sample is the highest. From 600 to 800 °C, the photocatalytic activity of the samples decreased as a function of temperature. It is widely accepted that the high calcination temperature usually results in larger particle sizes and smaller specific surface areas.³¹ This is not in favor of the photocatalytic

activity. In summary, this study identified 500 °C as the optimal calcination temperature.

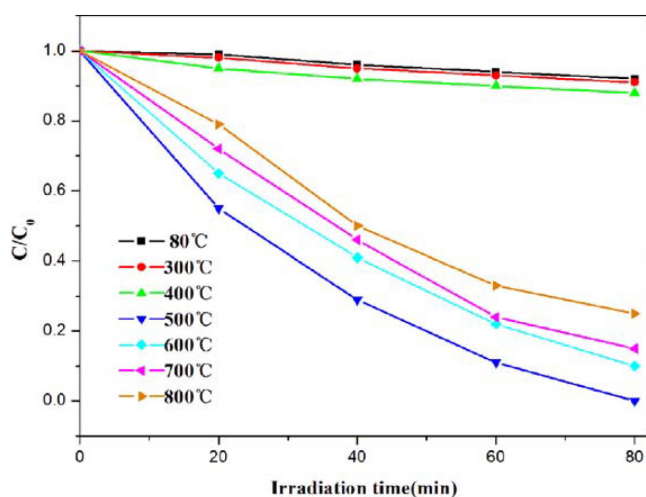


Figure 5. Photocatalytic activity as a function of calcination temperature of Cr/S/TiO₂-HGM as used to eliminate indigo carmine under visible light irradiation ($\lambda > 410$ nm)

The cycle of the photocatalyst

Stability is a crucial factor in the assessment and application of photocatalysts. To gain insight into the stability of the composite catalysts, we performed five consecutive recycling photocatalytic degradation tests on Cr/S/TiO₂-HGM samples under the same conditions. Initially, 0.6 g of Cr/S/TiO₂-HGM was dispersed in 100 mL of indigo carmine solution (20 mg L⁻¹). The mixture then underwent five consecutive cycles - each lasting 80 min. After each cycle, the photocatalyst was filtered, washed thoroughly with deionized water, and then added into fresh indigo carmine solution (20 mg L⁻¹).

The degradation efficiency of five consecutive cycles is shown in Figure 6. As cycling time increases, the catalytic properties of the Cr/S/TiO₂-HGM gradually decreased (Figure 6). The degradation rate in the second round was 98.06% versus 100% at baseline, but the efficiency was still 91.04% at cycle five. Therefore, the Cr/S/TiO₂-HGM photocatalyst is functionally stable for at least five rounds of photodegradation. Thus, the Cr/S/TiO₂-HGM has high cycle value. There is also a difference in the degradation rate of the indigo carmine solution by cycle 5. This is likely due to the Cr/S/TiO₂ photocatalytic degradation. Under visible irradiation, TiO₂ plays a role in indigo carmine degradation, the TiO₂ particle reacts with O₂, H₂O and/or OH⁻ to produced OH radicals, which degrade the indigo carmine. The reduced activity over time is due to Cr/S/TiO₂ shedding from the HGM surface.

The comparison of different materials photocatalytic activity

Figure 7 shows the photocatalytic activity of P25-TiO₂, Cr/S/TiO₂, Cr/S/TiO₂-HGM, and HGM as a function of visible light irradiation time. The HGM has negligible photocatalytic activity. The photocatalytic activity of P25-TiO₂ in visible light is very low, and it is well known that P25-TiO₂ does not absorb visible light. The Cr/S/TiO₂ and Cr/S/TiO₂-HGM have high photocatalytic activity under visible light. Compared Cr/S/TiO₂ with Cr/S/TiO₂-HGM, the Cr/S/TiO₂-HGM increases the specific surface area because of HGM. Thus, its photocatalytic activity is higher than the Cr/S/TiO₂. From a practical perspective, the powdered Cr/S/TiO₂ is not conducive to recycling, but the Cr/S/TiO₂-HGM effectively solves the problem.

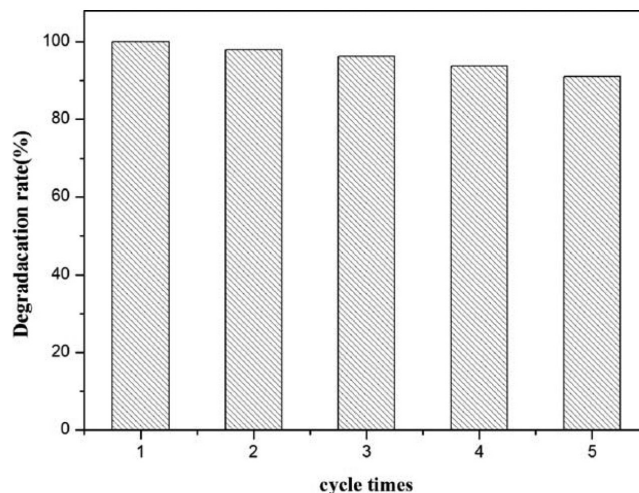


Figure 6. The degradation rate of indigo carmine by Cr/S/TiO₂-HGM as a function of cycle. Reaction time = 80 min ($\lambda > 410$ nm)

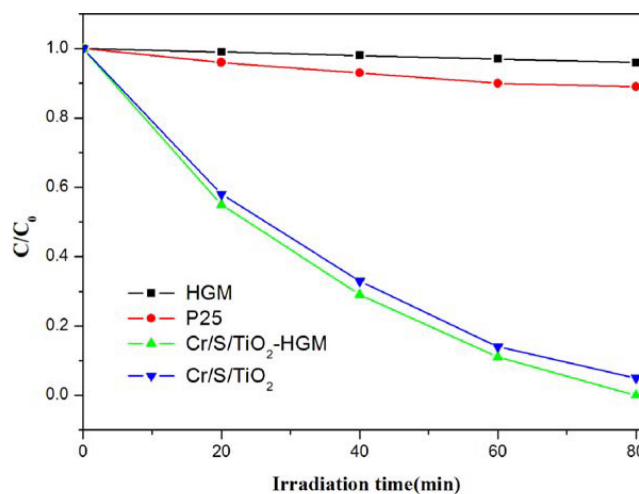


Figure 7. Photocatalytic activity of different materials used for the elimination of indigo carmine under irradiation with visible light ($\lambda > 410$ nm)

CONCLUSIONS

Hollow glass microspheres loaded with chromium and sulfur co-doped TiO₂ photocatalyst were synthesized by a sol-gel method. The Cr/S/TiO₂-HGM was evaluated in the degradation of indigo carmine under visible light. The Cr/S/TiO₂-HGM has superior photocatalytic performance under visible light irradiation. It can also be easily separated from the reaction system. This solves the problem of difficult recycling. Because of its enhanced visible light absorption, outstanding photocatalytic properties, and super recyclability, the Cr/S/TiO₂-HGM is promising for applications in the field of water treatment. The results provide a new method to identify powder catalyst loading.

ACKNOWLEDGEMENTS

The authors are grateful to Science Foundation of Ministry of Education of Heilongjiang Province (12511380).

REFERENCES

- Alahiane, S.; Qourzal, S.; Ouardi, M. E.; Belmouden, M.; Assabbane, A.; *J. Mater. Environ. Sci.* **2013**, *4*, 239.

2. Rauf, M. A.; Ashraf, S. S.; *Chem. Eng. J.* **2009**, *151*, 10.
3. Lakshmi, U. R.; Srivastava, V. C.; Mall, I. D.; Lataye, D. H.; *J. Environ. Manage.* **2009**, *90*, 710.
4. Jenkins, C. L.; *Arch. Environ. Health* **1978**, *40*, 7.
5. Jeffords, D. L.; Lance, P. H.; Dewolf, W. C.; *Urology* **1977**, *9*, 180.
6. Linsebigler, A. L.; Lu, G.; Yates, J. T.; *Chem. Rev.* **1995**, *95*, 735.
7. Zhang, X.; Liu, Q.; *Appl. Surf. Sci.* **2008**, *254*, 4780.
8. Lin, Y. H.; Tseng, T. K.; Chu, H.; *Appl. Catal., A* **2014**, *469*, 221.
9. Liu, S.; Feng, Q.; Tang, W.; *Chin. J. Inorg. Chem.* **2011**, *27*, 673.
10. Liu, S.; Tang, Q.; Feng, Q.; *Appl. Surf. Sci.* **2011**, *257*, 5544.
11. Chen, H.; Jin, H.; Dong, B.; *Res. Chem. Intermed.* **2012**, *38*, 2335.
12. Lu, Y.; Ni, L.; Yang, P.; Cao, Y.; *Chin. J. Catal.* **2007**, *28*, 987.
13. Jiang, W.; Joens, J. A.; Dionysiou, D. D.; *J. Photochem. Photobiol. A* **2013**, *262*, 7.
14. Merg, J. C.; Rossett, F.; Penha, F. G.; *Quim. Nova* **2010**, *33*, 1525.
15. Han, W.; Ren, L.; Zhang, Z.; *Ceram. Int.* **2015**, *41*, 7471.
16. Dos Santos, V. C.; Kondo, M. M.; *Quim. Nova* **2006**, *29*, 251.
17. Doumbia, A. S.; Bourmaud, A.; Jouannet, D.; *Polym. Degrad. Stab.* **2015**, *114*, 146.
18. Dalai, S.; Savithri, V.; Shrivastava, P.; *Int. J. Energ. Res.* **2015**, *39*, 717.
19. Ahn, K.; Kim, M.; Kim, K.; *J. Power Sources* **2015**, *276*, 309.
20. Ohno, T.; Akiyoshi, M.; Umabayashi, T.; Asai, K. T.; Matsumura, M.; *Appl. Catal., A* **2004**, *265*, 115.
21. Cong, Y.; Zhang, J.; Chen, F.; Anpo, M.; *J. Phys. Chem. C* **2007**, *111*, 6976.
22. Ren, W.; Ai, Z.; Jia, F.; Zhang, L.; Fan, X.; Zou, Z.; *Appl. Catal., B* **2007**, *69*, 138.
23. Sakatani, Y.; Ando, H.; Okusako, K.; *J. Mater. Res.* **2004**, *19*, 2100.
24. Sakatani, Y.; Nunoshige, J.; Ando, H.; *Chem. Lett.* **2003**, *32*, 1156.
25. Zhao, W.; Ma, W.; Chen, C.; Zhao, J.; Shuai, Z.; *J. Am. Chem. Soc.* **2004**, *126*, 4782.
26. Bonato, M. M.; Bragança, M. O. G. P.; Portella, K. F.; *Quim. Nova* **2014**, *37*, 1063.
27. Sun, B.; Reddy, E. P.; Smirniotis, P. G.; *Appl. Catal., B* **2005**, *57*, 139.
28. Dvoranova, D.; Brezova, V.; Mazur, M.; *Appl. Catal., B* **2002**, *37*, 91.
29. Liu, Z. L.; Cui, Z. L.; Zhang, Z. K.; *Funct. Mater.* **2005**, *36*, 1404.
30. Kato, H.; Kudo, A.; *J. Phys. Chem. B* **2002**, *106*, 5029.
31. Wang, Y.; Wang, Y.; Meng, Y.; *J. Phys. Chem. C* **2008**, *112*, 6620.